

# The *XMM-Newton* slew survey in the 2–10 keV band

R.S. Warwick<sup>1</sup>, R.D. Saxton<sup>2</sup>, and A.M. Read<sup>1</sup>

<sup>1</sup> Dept. of Physics and Astronomy, University of Leicester, Leicester LE1 7RH, U.K.

e-mail: rsw@star.le.ac.uk

<sup>2</sup> XMM SOC, ESAC, Apartado 78, 28691 Villanueva de la Cañada, Madrid, Spain

Received; accepted

## ABSTRACT

**Context.** The on-going *XMM-Newton* Slew Survey (XSS) provides coverage of a significant fraction of the sky in a broad X-ray bandpass. Although shallow by contemporary standards, in the “classical” 2–10 keV band of X-ray astronomy, the XSS provides significantly better sensitivity than any currently available all-sky survey.

**Aims.** We investigate the source content of the XSS, focussing on detections in the hard 2–10 keV band down to a very low threshold ( $\geq 4$  counts net of background). At the faint end, the survey reaches a flux sensitivity of roughly  $3 \times 10^{-12}$  erg cm<sup>-2</sup> s<sup>-1</sup> (2–10 keV).

**Methods.** Our starting point was a sample of 487 sources detected in the XSS (up to and including release XMMSL1d2) at high galactic latitude in the hard band. Through cross-correlation with published source catalogues from surveys spanning the electromagnetic spectrum from radio through to gamma-rays, we find that 45% of the sources have likely identifications with normal/active galaxies. A further 18% are associated with other classes of X-ray object (nearly coronally active stars, accreting binaries, clusters of galaxies), leaving 37% of the XSS sources with no current identification. We go on to define an XSS extragalactic sample comprised of 219 galaxies and active galaxies selected in the XSS hard band. We investigate the properties of this extragalactic sample including its X-ray log N - log S distribution.

**Results.** We find that in the low-count limit, the XSS is, as expected, strongly affected by Eddington bias. There is also a very strong bias in the XSS against the detection of extended sources, most notably clusters of galaxies. A significant fraction of the detections at and around the low-count limit may be spurious. Nevertheless, it is possible to use the XSS to extract a reasonably robust sample of extragalactic sources, excluding galaxy clusters. The differential log N - log S relation of these extragalactic sources matches very well to the HEAO-1 A2 all-sky survey measurements at bright fluxes and to the 2XMM source counts at the faint end.

**Conclusions.** The substantial sky coverage afforded by the XSS makes this survey a valuable resource for studying X-ray bright source samples, including those selected specifically in the hard 2–10 keV band.

**Key words.** Surveys – X-rays: general – Galaxies:active

## 1. Introduction

One of the on-going programmes of *XMM-Newton* is a shallow large-area X-ray survey based on data recorded by the on-board cameras as the observatory slews from one target source to the next. The first catalogue of *XMM-Newton* Slew Survey sources (XMMSL1) was released in May 2006 and then updated in August 2007 (XMMSL1d1). Later additions to the catalogue were made in April 2008 (XMMSL1d2), July 2009 (XMMSL1d3), April 2010 (XMMSL1d4) and most recently June 2011 (XMMSL1d5). The full *XMM-Newton* slew catalogue is available from the *XMM-Newton* Science Archive (XSA).

As discussed by Saxton et al. (2008), the *XMM-Newton* Slew Survey (hereafter XSS) is based solely on data from the EPIC pn camera, since the longer readout times of the MOS cameras lead to a very elongated point spread function in slew observations. The in-orbit slew speed of 90 degrees per hour results in an exposure time for sources lying on the slew path of between 1–11s. The XSS records the count rates of sources in two nominal energy ranges, namely a “soft” 0.2–2 keV band and a “hard” 2–12 keV band. In practice, the high energy fall-off in the pn detector response results in a negligible contribution to the XSS source count rates from X-ray photons with energies between 10–12 keV and, hereafter, we take the energy range of the XSS hard band to be 2–10 keV.

In the soft 0.2–2 keV band the limiting sensitivity for source detection in the XSS is roughly  $6 \times 10^{-13}$  ergs cm<sup>-2</sup> s<sup>-1</sup>, which is very comparable to that reached in the ROSAT All-Sky Survey (RASS; Voges et al. 1999). In the hard 2–10 keV band the limiting sensitivity for source detection is approximately  $3 \times 10^{-12}$  ergs cm<sup>-2</sup> s<sup>-1</sup>. This is roughly an order of magnitude deeper than the *all-sky* surveys which are currently available in this energy range, such as those from *Uhuru*, *Ariel V*, and *HEAO-1* (Forman et al. 1978; McHardy et al. 1981; Piccinotti et al. 1982; Wood et al. 1984). The situation is, of course, very different if one considers surveys with sky-coverage much less than  $4\pi$  steradians. This includes the low/medium depth surveys from ASCA (Ueda et al. 2005) and BeppoSax (Giommi, Perri & Fiore 2000), the multi-observation dedicated surveys and serendipitous observations carried out by *XMM-Newton* and *Chandra* (e.g., Mateos et al. 2008; Elvis et al. 2009) and the ultra-deep pencil-beam surveys also completed by these latter two missions (e.g., Alexander et al. 2003; Luo et al. 2008; Xue et al. 2011; Brunner et al. 2008; Comastri et al. 2011). These recent surveys reach sensitivity levels three orders of magnitude fainter than the XSS.

Within this setting, the XSS survey has two important attributes: (i) the coverage of a relatively large sky area (35% of the sky up to and including the XMMSL1d2 release considered here, rising to 52.5% with the most recent increments) and (ii)

the sampling of a flux range in the hard band for which current source catalogues provide far from comprehensive information. At the high flux end, the XSS overlaps with the existing all-sky 2–10 keV surveys, whereas at its sensitivity limit, the XSS is detecting objects which are still “X-ray bright” in the context of the targeted *XMM-Newton* programme. Although well represented in the 2XMM catalogue (Watson et al. 2009), the use of this catalogue (or similar catalogues) to evaluate the statistical properties of “bright” sources is greatly complicated by the complex biases and selection effects, which necessarily influence the target and field selection of an observatory-class mission (Mateos et al. 2008).

In this paper we explore the statistical properties of the XSS, focussing on sources detected in the hard band. More specifically we investigate the extragalactic component of the XSS catalogue. In the next section, we describe the criteria used to select our source sample, examine some of the basic properties of the XSS sources, investigate the likely false detection rate and also explore the strong bias against the detection of extended sources. In §3 we describe the results of a cross-correlation of the XSS source positions with published source catalogues spanning a wide range of wavebands and where possible categorize each source on the basis of the type of counterpart. We then go on in §4, to explore the multiwavelength properties of an XSS hard-band selected sample of extragalactic sources (excluding galaxy clusters). In §5 we construct the log N - Log S distribution of the extragalactic sample utilizing the results from a simulation of the survey process. We then discuss the degree to which our XSS source sample bridges the gap in flux coverage between the “classical” 2–10 keV all-sky surveys and the current generation of deep pointed-mode surveys. Finally in §6 we provide a brief summary of our conclusions.

## 2. The XSS hard-band selected sample

### 2.1. Definition of the source sample

Full details of the procedures used to construct a source catalogue based on *XMM-Newton* slew data are reported in Saxton et al. (2008). Our starting point was the “clean” version of the XSS catalogue based on slews performed up to Jan. 2008 (XMMSL1d2), which contains a total of 7686 sources (compared to the 2692 “clean” sources reported by Saxton et al. based on a more limited set of slew observations).

When we select only those sources detected in the XSS hard band<sup>1</sup>, there is a dramatic drop to 796 catalogue entries. A further requirement that sources be located well off the Galactic Plane, with  $|b| > 10^\circ$ , results in a “preliminary” list of 617 hard-band selected sources. The total area of high-latitude sky encompassed by the slew observations was 14233 square degrees, but after allowing for overlaps this figure reduced to 11914 square degrees (*i.e.*, 35% coverage of the sky region above  $|b| > 10^\circ$ ).

The next step was to filter the source sample on the basis of various parameters recorded in the XSS database. Selection criteria were set as follows: (i) a minimum net source count of 4 (*i.e.*, the number of counts assigned to the source after background subtraction); (ii) a minimum hard-band count rate of 0.4

ct/s; (iii) a minimum effective exposure time of 1 s and (iv) a maximum source extent of 15 pixels ( $\approx 60''$ ). Application of these criteria reduced the sample to 540 sources. We further applied a cut on the maximum count rate of 10 ct/s; this serves as a precaution against pile-up effects in the detector but also proved a useful upper bound in the investigation of the source number counts. This removed detections of 4 well-known active galactic nuclei (AGN), namely Mrk421, IC4329A, NGC5506 and 3C390.3, 16 bright Galactic X-ray binary sources and one likely spurious source. The result was a sample of 519 sources detected in the pn camera with count rates in the range 0.4–10 ct/s. The next consideration was duplicate detections of the same source. There were 30 duplicates and one example of a triple detection in our list. We excluded duplicates by selecting the source detection with the highest maximum likelihood in the XSS hard band<sup>2</sup>. With the duplicates removed, our final sample consisted of 487 hard-band selected sources.

Some of the properties of this XSS source sample are illustrated in Fig. 1, where a distinction is made between the full sample and the subset of the XSS sources which were detected solely in the hard band (see §2.2 for further consideration of this issue). The bulk of the sources have exposure times in the range 2–10s (Fig. 1a). The distribution of the counts recorded in the hard band (after background subtraction) is strongly weighted towards the 4-count limit with 194 sources having between 4–5 net counts (Fig. 1b). Fig. 1c shows that the net counts and the maximum likelihood for the detection are, as expected, well correlated, albeit with a significant scatter. Finally Fig. 1d shows the relation between the net counts and the derived count rate; here the impact of the factor of 5 spread in the effective exposure time is apparent in terms of the commensurate spread in the count rate at a given net count.

If we assume a source spectral model comprising a power-law continuum with photon index  $\Gamma = 1.7$  with soft X-ray absorption equivalent to a column density  $N_H = 3 \times 10^{20} \text{ cm}^{-2}$ , then the count rate to flux conversion is  $1 \text{ ct/s} = 8.1 \times 10^{-12} \text{ erg s}^{-1} \text{ cm}^{-2}$  (2–10 keV) for the medium filter. Our XSS hard-band selected sample therefore includes sources with 2–10 keV fluxes broadly in the range  $0.3\text{--}8 \times 10^{-11} \text{ erg s}^{-1} \text{ cm}^{-2}$ .

### 2.2. Concurrent hard- and soft-band detection

In addition to the 2–10 keV measurements, the XSS also provides soft band (0.2–2 keV) data. Just over half (254 sources out of 487) of the hard-band selected sources were also detected simultaneously in the XSS soft band. Fig. 2 shows a comparison of the count rates measured in the two XSS bands for the sources in our sample. In this figure the lower and upper diagonal lines represent soft:hard count-rate ratios of 1:1 and 10:1 respectively. For a source spectral model comprising a power-law continuum with  $\Gamma = 1.7$  subject to soft X-ray absorption equivalent to  $N_H = 3 \times 10^{20} \text{ cm}^{-2}$  (the fiducial spectral form on which the count rate to flux calibration is based), the soft to hard count-rate ratio is  $\approx 2.7$ . This ratio increases to over 10 for  $\Gamma \approx 2.5$ ; similarly it drops to below 1 if the column density is increased to  $N_H \approx 5 \times 10^{21} \text{ cm}^{-2}$  (for  $\Gamma = 1.7$ ).

### 2.3. False detections in the XSS

A survey which extends to sources with only 4 net counts, measured against a low but not entirely negligible background,

<sup>1</sup> For a source to be included in our sample we require a detection maximum likelihood (*maxl*) in the XSS hard band of either *maxl* > 10, if the background count rate was less than 3 ct/s, or *maxl* > 14 otherwise. These are the same criteria as used to define the “clean” XSS sample, except now applied specifically to the hard band. Note that in the on-line XSS catalogue the *maxl* parameter has the designation DET\_ML.

<sup>2</sup> Note that a duplicate detection of Mrk 421 at a count rate less than the 10 ct/s upper threshold, restored this source to our final sample.

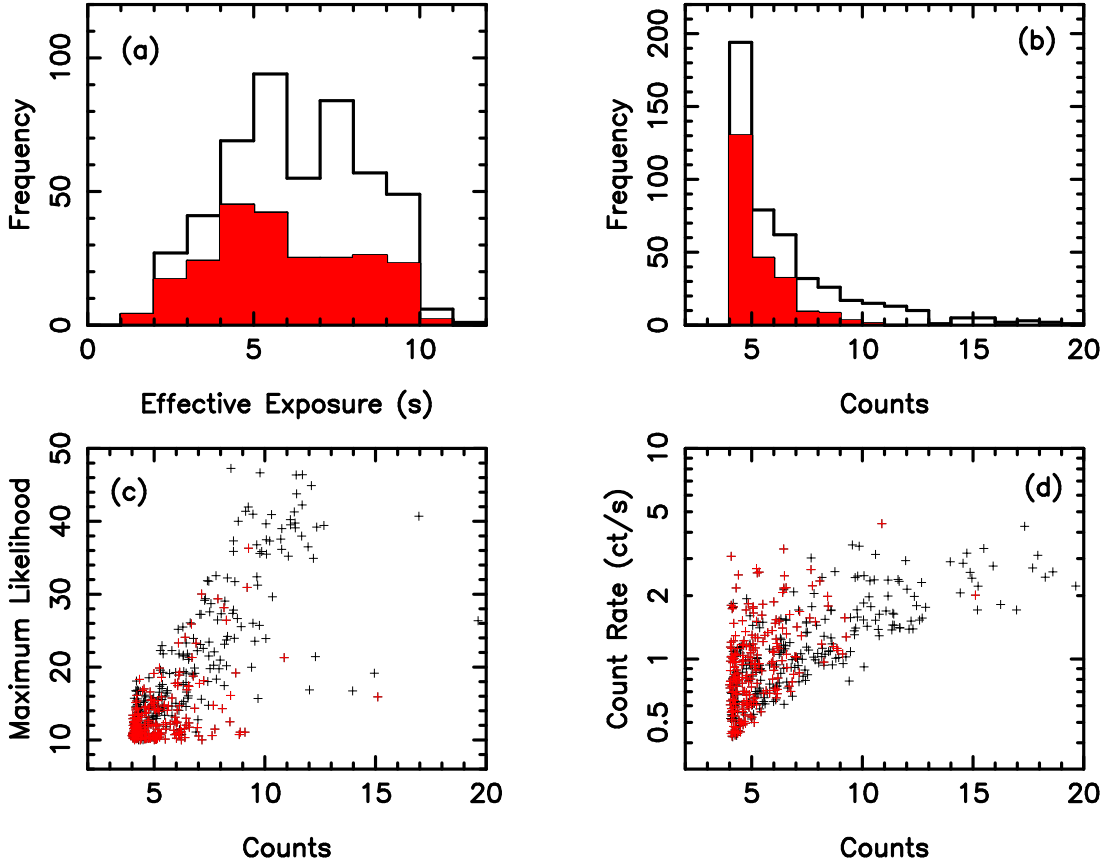


**Fig. 1.** Characteristics of the 487 sources comprising the XSS hard-band selected sample. *Panel (a):* Distribution of the effective exposure time of the full sample. The filled (red) histogram corresponds to the subset of XSS sources which were detected only in the XSS hard band. *Panel (b):* Distribution of the net counts recorded in the hard (2–10 keV) band (after background subtraction). The filled (red) histogram again corresponds to the hard-band only sources. *Panel (c):* Net counts versus the maximum likelihood of the detection with the hard-band only sources plotted in red. *Panel (d):* Net counts versus the corresponding count rate in ct/s with the hard-band only sources plotted in red. For clarity the 20 sources with net hard counts in the range 20–70 are not shown in *Panels (b)–(d)*.

will include some false detections arising from Poissonian noise spikes. In the case of the XSS sample one would expect the vast majority of the false detections to reside amongst the sources detected only in the hard band (since the probability of a simultaneous false detection in both the hard and soft bands will be very small). It is certainly true that the subset of “hard-band only” sources has a somewhat stronger weighting towards low net counts than the sources detected in both bands (see Fig. 1b). Specifically, 130 out of 233 (56%) of the hard-band only sources have between 4–5 net hard-band counts compared to 64 out of 254 (25%) for the dual-band detections.

To obtain an estimate of what fraction of the 233 XSS sources detected only in the hard-band might actually be spurious detections, we have applied the following argument. If we crudely approximate the source detection process (ignoring any issues relating to the background subtraction) as a search for groupings of  $N$  or more counts within a source cell of radius  $R = 20''$ , then there are approximately  $1.4 \times 10^8$  such cells over the full XSS survey region. The typical background count in such a cell, based on the actual backgrounds measured in the XSS images, was in the range 0.01–0.05 counts, for which the Poissonian probability of measuring  $N \geq 4$  is roughly  $1.0 \times 10^{-7}$  (applying a weighted average over the background distribution). This

implies the detection of just 14 spurious sources. The predicted false detection rate increases rapidly with  $R$ , with  $R = 30''$  giving roughly 150 false detections (although this is probably an overestimate of the effective source cell size). A further observation is that the low-count sources are not preferentially drawn from slew datasets with higher than average background; this suggests that if there is a high false detection rate amongst such sources, then then its origin is not solely due to Poissonian background fluctuations.

As a further test we randomised the photon distribution in a subset of the slew survey images and reran the source search algorithm. After applying the same selection criteria as employed in the current study, the number of spurious source detections, scaled to the full XSS area, was 33. However, we note that this approach does not encompass all of the complexities of the source detection within the XSS.

We will return to this issue when we consider the high number of “unidentified” sources amongst the subset of sources detected only in the XSS hard band.

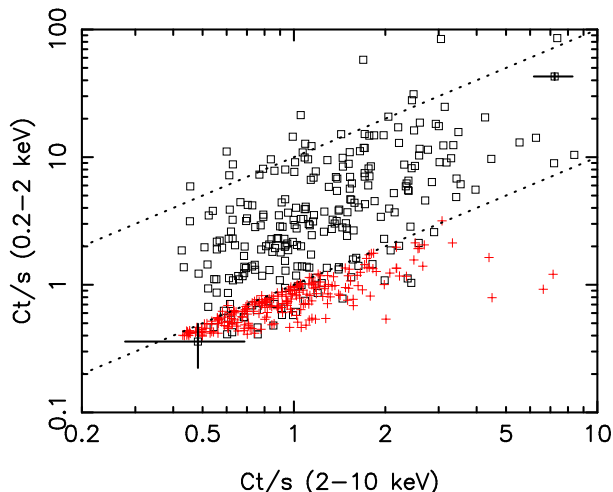


**Fig. 2.** XSS soft-band (0.2-2 keV) count rate versus the hard band (2-10 keV) count rate. Sources detected in both the hard and soft bands are plotted as squares, whereas those for which the soft-band measurement is an upper limit (corresponding to 4 net counts) are shown as (red) pluses. Error bars are shown for one high and one low-count rate source for illustration. The dotted diagonal lines correspond to soft to hard count-rate ratios of 1:1 and 10:1.

#### 2.4. Bias against the detection of extended sources

Some of the difficulties relating to the detection of extended sources in the low-exposure, low-count regime of the XSS have been discussed by Saxton et al. (2008). In practice, these issues translate to a fairly strong bias against the inclusion of extended objects within the current XSS sample. This selection bias will particularly impact on X-ray sources associated with nearby clusters of galaxies, which form a substantial fraction of the high-latitude source population seen in *all-sky* surveys such as *Uhuru*, *Ariel V*, and *HEAO-1*.

In selecting our XSS sample we imposed an upper limit on the extent parameter of 15 pixels ( $\approx 60''$ ). However, when we relax this selection criterion, the total number of sources in the sample only increases by six, none of which are obvious cluster candidates. Given this outcome, it is clear that the bias against extended objects is an intrinsic feature of the XSS.

To illustrate the magnitude of the problem, we have employed the complete sample of high-latitude ( $|b| > 20^\circ$ ) sources detected by the *HEAO 1* A-2 experiment in the 2–10 keV band (Piccinotti et al. 1982) as a comparator. This sample (which we hereafter refer to as the Piccinotti sample) comprises 68 sources, 30 of which are identified as clusters of galaxies. We have investigated whether the XSS encompasses the positions of each of the Piccinotti sources and, where there is coverage, whether a hard-band detection resulted. For the non-detections we have gone back to the slew-survey data and determined an upper limit using a Bayesian-based on-line tool (Saxton & Gimeno 2011).

The results of this investigation were as follows. Ten of the Piccinotti clusters were covered by the XSS (up to and including XMMSL1d2). Of these 3 appear in our current sample with extent parameters in the range 3-14 pixels. A further *HEAO 1* A-2 cluster was detected with an extent parameter of 20 pixels (but in the event this source did not make it into the XSS “clean” sample which was the starting point of our selection process). The X-ray fluxes derived for these 4 objects from the XSS were

comparable (within a factor  $\sim 2$ ) with those measured by the *HEAO 1* A-2 experiment. The remaining 6 clusters were not detected with upper-limits (assuming point-like sources) between 3-30 times lower than those predicted from the *HEAO 1* A-2 fluxes. As a further comparison the same analysis carried out for the 12 AGN in the Piccinotti sample covered by the XSS gave 10 detections plus 2 upper-limits with inferred variability factors typically in the range 1-3.

We conclude from this analysis that a strong bias does exist against the detection of extended objects in the XSS.

### 3. Counterparts to the XSS sources

#### 3.1. Identification process

The next step was to draw together the available multiwavelength information relating to the likely counterparts of the sources in our XSS hard-band selected sample. The starting point was the cross-correlation of the XSS positions with other source catalogues encompassing a wide wavelength range. Saxton et al. (2008) quote the typical astrometric uncertainty of XSS positions to be  $8''$  (the 68% confidence error radius), but for the purpose of cross-correlation with other catalogues, we initially adopted a search radius of  $30''$ . This process relied heavily on the facilities of Vizier<sup>3</sup>, supplemented by reference to Simbad<sup>4</sup> and NED<sup>5</sup>. A few catalogues not currently available at Vizier were also accessed directly from the survey websites, the most notable being the Sloan Digital Sky Survey SDSS<sup>6</sup> and the Galaxy Evolution Explorer, GALEX<sup>7</sup>, source catalogues. In a preliminary pass we made a judgement on the likely identification of the X-ray source, if any. In the great majority of cases this involved consideration of the available information for a single putative counterpart, although in a small number of instances it was necessary to select the most likely counterpart amongst two or three candidates (using criteria such as the offset from the X-ray position and the brightness of the sources).

This first iteration separated the XSS sample into six broad categories. Sources of likely extragalactic origin were flagged as either *AGN*, *Galaxies* or *Clusters* (of galaxies). In general sources were categorized as *Galaxies* rather than *AGN* when there was a report of an extended optical/IR morphology and/or an associated redshift, but no definitive confirmation of the presence of an active nucleus. Similarly objects of likely Galactic origin were divided into *Stars* (mostly nearby objects with active stellar coronae) and *Other* categories (including X-ray binaries, cataclysmic variables supernova remnants and one pulsar). X-ray sources most likely residing in Local Group galaxies (M31, LMC and SMC) were also assigned to the *Other* category, as was an Ultraluminous X-ray Source (ULX) detected NGC 2403. Finally the XSS sources without an obvious counterpart were categorized as *Unidentified*.

Subsequent iterations allowed the refinement of the above process using the knowledge derived from the earlier cycle. In particular, the great majority of the sources categorized as either the *AGN*, *Galaxies* or *Stars* were found to have both near-

<sup>3</sup> <http://vizier.u-strasbg.fr/viz-bin/VizieR/>

<sup>4</sup> <http://simbad.u-strasbg.fr/simbad/>

<sup>5</sup> <http://ned.ipac.caltech.edu/>

<sup>6</sup> <http://www.sdss.org/>

<sup>7</sup> <http://galex.stsci.edu/galexview/>

**Table 1.** Division of the XSS sample into source types.

Source Type	All	Hard+Soft	Hard-only
AGN	181	160	21
Galaxies	38	16	22
Clusters	10	10	0
Stars	53	51	2
Other	27	17	10
Unidentified	178	0	178 <sup>¶</sup>
Total	487	254	233

<sup>¶</sup> This includes the 68 hard-only sources with  $pos\_err > 10''$  which were not formally included in the identification process.

IR and mid-IR counterparts in the 2MASS<sup>8</sup> and WISE<sup>9</sup> surveys respectively. This allowed both the astrometric precision of the XSS and the IR colours of the counterparts to be explored in a systematic way. One application of the latter was to resolve some initial ambiguity as to whether the likely counterpart was a galaxy or a star on the basis of its IR colour (see §4.2). Also by exploiting the GALEX survey (Martin et al. 2005), which currently provides UV coverage of roughly two-thirds of the sky in the near-UV (NUV, 1350–1750 Å) and far-UV (FUV, 1750–2750 Å) bands, a number of sources initially categorized as *Galaxies* were switched to *AGN* on the basis of their UV to near-IR colour (§4.1).

An important consideration emerged in relation to the subset of XSS sources which were detected only in the hard X-ray band. Hereafter we refer to this subset as the “hard-only” sources, as opposed to the “hard+soft” sources detected simultaneously in both XSS bands. For the hard-only sources the success rate in finding relatively bright, plausible counterparts within a nominal search radius proved to be surprisingly low. As a consequence, in searching for putative counterparts down to fainter magnitudes, the rate of chance coincidences emerged as a crucial issue. In the event it proved necessary to focus on the hard-only sources with reasonable position errors as defined by the XSS  $pos\_err$ <sup>10</sup>. As a practical approach the 68 hard-only sources with  $pos\_err > 10''$  were excluded from the identification statistics, although in practice there were very few plausible counterparts amongst this group. As a further step rather tight constraints were placed on the positional offsets and limiting magnitudes of the objects considered to be plausible counterparts to the remaining hard-only sources (see §3.3 for further details).

A summary of the final identification statistics for the full XSS sample is provided in Table 1, where the division is into the six broad source categories defined earlier. Table 1 also provides the identification information split down to the hard+soft and hard-only source subsets.

<sup>8</sup> The Two Micron All Sky Survey (2MASS) (Cutri et al. 2003; Skrutskie et al. 2006) provides uniform coverage of the entire sky in three near-infrared (NIR) bands, namely in J (1.25 $\mu$ ), H (1.65 $\mu$ ) and K<sub>s</sub> (2.17 $\mu$ ).

<sup>9</sup> The Wide Field Infrared Explorer (WISE) has recently observed the entire sky at 3.4, 4.6, 12 and 22  $\mu$ m. The All-SKY Data Release covers > 99% of the sky and incorporates the best available calibrations and data reduction algorithms (Cutri et al. 2012).

<sup>10</sup> The  $pos\_err$  parameter provides an estimate of the uncertainty of the XSS position, albeit a rather crude one for sources at the low-count threshold. In the present work we restrict its use to filtering out the hard-only sources with particularly poor position determinations. Note that in the on-line XSS catalogue the  $pos\_err$  parameter has the designation RADEC\_ERR.

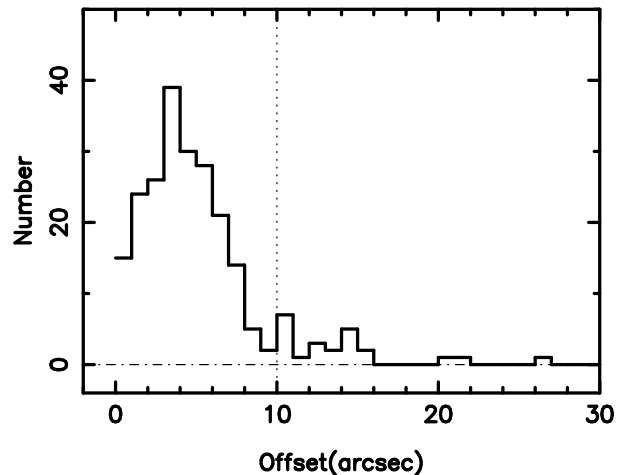


**Fig. 3.** X-ray to counterpart positional offsets for the XSS hard+soft sources classed as either AGN, Galaxies or Stars. The dotted vertical line is drawn at 10'' and represents a nominal 90% error circle radius.

### 3.2. Counterparts of the XSS hard+soft sources

We first consider the identification statistics for the XSS sources detected simultaneously in both the XSS hard and soft bands (Table 1, col.3). A striking result is potential counterparts can be identified for *all* of these sources. Rather as expected, AGN predominate, whereas the number of clusters is small, consistent with our earlier discussion of the strong bias against extended sources in the XSS survey.

Within the hard+soft subset, 227 sources (out of 254) are categorized as either *AGN*, *Galaxies* or *Stars*. Of these, 223 appear in the WISE catalogue. For the four remaining sources, potential identifications were found in the GALEX catalogue (3 sources) or in 2MASS (a bright star); hence we have a complete set of counterpart positions for the *AGN*, *Galaxies* and *Stars*. The distribution of the angular offsets between the XSS position and the counterpart position is shown in Fig. 3. From this distribution one can conclude that the XSS 68% error radius is at  $\approx 6''$  (which may be compared to the earlier estimate of 8'' quoted by Saxton et al. 2008) and the 90% XSS error radius is at  $\approx 10''$ . Beyond 10'' the offset distribution exhibits a long tail (Fig. 3), which might perhaps point to some of the identifications being incorrect. By way of illustration, consider the three most extreme outliers for which the putative counterpart is offset from the XSS position by  $> 20''$ . In these cases, the proposed counterparts (1 star, 1 galaxy and 1 AGN) are all relative bright WISE sources and are the only candidates visible within 30'' of the X-ray position. Assuming that in these cases and in the others comprising the tail of the offset distribution, we do have the correct identification, then it would appear that the XSS position determination is occasional subject to atypical systematic errors (of up to 20''), the origin of which are unknown.

As noted previously, the great majority of sources classed as either *AGN*, *Galaxies* or *Stars* have counterparts visible in both the 2MASS near-IR and the WISE mid-IR catalogues. There are in fact 213 hits with 2MASS and 223 with WISE out of a total sample of 227 objects. Fig. 4 shows the resulting magnitude distributions for both the 2MASS J band and the WISE W1 (3.4  $\mu$ m) band, with the contribution of objects classed as *Stars* highlighted. Clearly nearby stars dominate at bright mag-

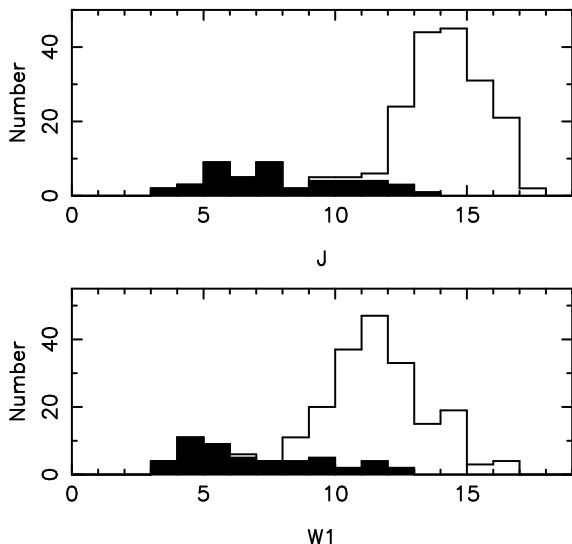


**Fig. 4.** *Upper panel:* The 2MASS J magnitude distribution of the counterparts to the XSS hard+soft sources categorized as either *AGN*, *Galaxies* or *Stars*. *Lower panel:* The WISE W1 (3.4  $\mu\text{m}$ ) magnitude distribution for the same source classes. In both panels the contribution of the *Stars* is highlighted as the filled histogram.

nitudes in both the near- and mid-IR. The broad J magnitude distribution of the coronally active stars detected in the XSS, with a shallow peak around  $J = 5-8$ , is in line with the much fainter ( $J \approx 13 - 16$ ) population of such objects discovered serendipitously in pointed *XMM-Newton* observations at X-ray flux levels  $\sim 10^3$  times fainter than those reached in the XSS (see Warwick, Pérez-Ramírez & Byckling 2011). The overlap region, between the stars on the one hand and AGN/galaxies on the other, extends over roughly 5 magnitudes in both the J and W1 bands demonstrating that the apparent brightness of the counterpart is not a particularly effective method of distinguishing between Galactic and extragalactic counterparts. The peak in magnitude distribution for the *AGN* and *Galaxies* is well above the limiting sensitivity of both the 2MASS and WISE surveys, indicating that at the X-ray flux levels sampled by the XSS, these two surveys provide an ideal starting point for source identification.

### 3.3. Counterparts of the XSS hard-only sources

It is immediately evident from Table 1 (col.4) that the success rate in finding potential identifications for the XSS sources detected solely in the hard band is very much lower than that of sources detected simultaneously in both the XSS bands. The large number of sources which remain unidentified in the hard-only subset clearly merits some investigation.

A first consideration is that the XSS hard-only sources will have poorer position determinations than the hard+soft by virtue of the smaller number of counts available for the position determination algorithm (we employ the “best” XSS positions which, in most cases, derive from all the available counts for any given source). As noted earlier, to mitigate the impact of the poorer positions, we excluded hard-only sources with  $pos\_err > 10''$  from the identification statistics. The net effect of the  $pos\_err$  constraint was to reduce the hard-only sample from 233 sources to

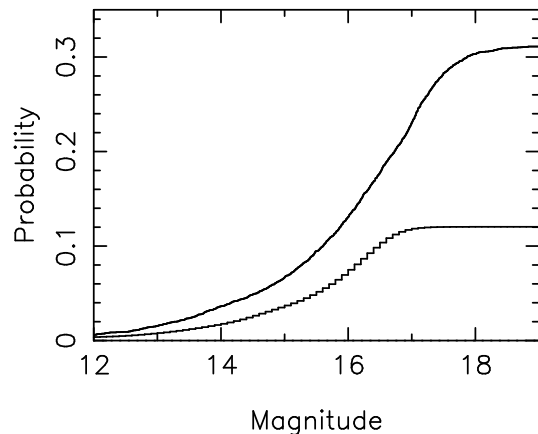


**Fig. 5.** The probability of finding by chance an object brighter than a given magnitude within a  $10''$  radius error circle. The upper curve corresponds to the WISE W1 (3.4  $\mu\text{m}$ ) band and the lower curve to the 2MASS J band.

165 sources. For comparison, if the same filter were to be applied to the hard+soft sources this would lead to the removal of just 8 sources, 5 of which lie in the *Clusters* category.

Even with the reduced sample, a large fraction of the hard-only sources remain unidentified (110 out of 165, *i.e.* two-thirds of the sample). With so many unidentified sources, it was essential to take account of the chance coincidence rate when searching for potential counterparts down to relatively faint fluxes. To quantify this we investigated the probability of finding an object within a nominal  $10''$  error circle as a function of the limiting magnitude for both the 2MASS J and the WISE W1 bands. In both cases the chance rates were determined by searching for the brightest object within a  $10''$  circle positioned at a set of grid points around each XSS source location (with an offset from the actual X-ray position always  $> 1'$ ). The results are shown in Fig.5. It is evident that at the survey limit, the WISE W1 band probes a source density  $\approx 2.6$  times higher than that reached in the 2MASS J band. Therefore, in the analysis below, we use the WISE survey as our yardstick for determining the chance coincidence rate.

Setting aside the 10 sources in the *Other* category, we conducted a systematic search for the counterparts to the hard-only sources using the WISE survey. For putative counterparts brighter than  $W1 = 12$  we extended the search radius to  $20''$ , whereas for objects in the range  $W1 = 12-15$  we restricted the radius to  $10''$  (noting that the latter equates to the 90% error radius for the hard+soft sources). Candidate objects fainter than  $W1 = 15$  were not considered. The number of potential counterparts as a function of the W1 magnitude emerging from this process is listed in Table 2, together with an estimate of the number of source expected by chance across the 165 sources comprising the (reduced) hard-band only sample. In total 45 potential counterparts were found - as reported in Table 1. The corresponding number of chances coincidences was predicted to be 10.6. We note from Table 2 that at the faint end of the magnitude range considered, the chance rate is rapidly approaching the actual number of objects found. We conclude, that a limiting W1 magnitude of  $\approx 15$  and a search radius at faint fluxes of no more than  $10''$  defines a reasonable bound to counterpart searches for the hard-only XSS sample.

**Table 2.** Incidence of potential WISE counterparts amongst the 165 sources comprising the (reduced) hard-only sample as a function of the W1 (3.4  $\mu\text{m}$ ) magnitude.

W1 magnitude	Search Radius (arcsec)	No. of Counterparts	Chance Rate
<10	20	2	1.0
10-11	20	9	1.2
11-12	20	17	1.4
12-13	10	5	1.2
13-14	10	7	2.4
14-15	10	5	3.4
Total		45	10.6

Of the 45 hard-only sources classed as *AGN*, *Galaxies* or *Stars*, only 2 fall in the latter category. This presumably reflects the fact that coronally active stars generally have soft thermal spectra and are not subject to significant line-of-sight absorption (particularly when detected at high Galactic latitude). The split between *AGN* and *Galaxies* is also much more strongly weighted to the latter in the hard-only sample. This could be the result of absorbing material within the host galaxy suppressing both the soft X-ray emission and also masking the *AGN* character of the source at longer wavelengths.

This leaves us with some uncertainty as to the nature of the numerous unidentified sources in the hard-only sample. If one applies the same filtering to the hard+soft identification as applied to the hard-only sources ( $pos\_err < 10''$ ,  $W1 < 15$ , search radii as in Table 2), then the number of sources (*AGN*, *Galaxies* and *Stars*) with putative WISE counterparts drops from 233 to 205, *i.e.*, a modest 12% decrease. It would seem that the unidentified sources amongst the hard-only sample, if real, must represent a population of astrophysical sources substantially fainter than found amongst the XSS hard+soft subset. However, there is no real evidence for the emergence of such a population down to  $W1=15$ , which is 3 magnitudes fainter than the peak of distribution in Fig.4. One might speculate that the unidentified sources correspond to infrequent, relatively short-lived outbursts linked to an otherwise underluminous source population, but in truth they are difficult to match to any known class of X-ray emitting object (see also §5.2). Unfortunately, a follow-up study of a subset of XSS sources with SWIFT provided no information contrary to the above analysis (Starling et al. 2011).

The alternative possibility is that a great many of the unidentified sources are not real astrophysical sources, but rather false detections, mostly at the 4-count threshold. The argument against this hypothesis is that the numbers of sources involved exceed the estimates of §2.3 by a factor of at least 3. However, given the nature of the XSS, a higher than predicted false detection rate is certainly a possibility. At the very least some caution is needed when dealing with XSS sources detected only in a single band at the 4-count limit.

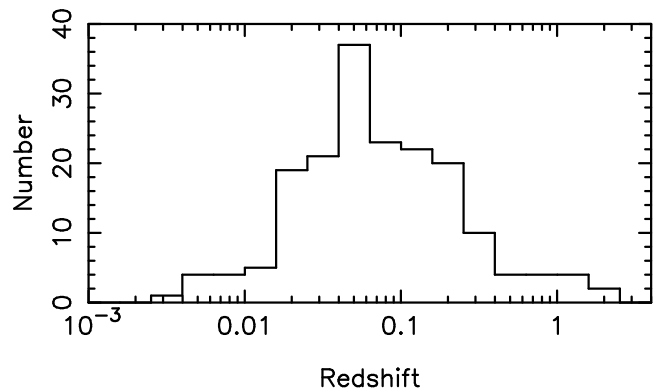
## 4. The XSS extragalactic sample

### 4.1. Composition of the sample

We may now use the source identifications to construct an XSS extragalactic sample. To this end, we have included the sources classed as either *AGN* or *Galaxies* in Table 1, but excluded *Clusters* given the strong bias against such sources in the XSS. Our full XSS extragalactic sample comprises 219 sources.

**Table 3.** Division into source types in the XSS extragalactic sample

Type	Full Sample	Hard+soft Subset	Hard-only Subset
Liner	2	2	0
Sy 1-1.5	79	73	6
Sy 1.9-2	14	7	7
RG/QSO	40	35	5
BLLac	28	27	1
UVX	18	16	2
Galaxy	38	16	22
Total	219	176	43

**Fig. 6.** Redshift distribution of the sources in the XSS extragalactic sample. Redshifts are known for 181 out of the 219 sources which comprise the sample.

Details of the individual sources are provided in the appendix (Table A.1), where we list the counterpart position, source type and redshift (if known).

The composition of the extragalactic sample is presented in Table 3 for the full set of sources and also split between the hard+soft and hard-only subsets. Here the *AGN* are grouped according to their spectroscopic classification, as taken from the literature. As noted earlier a number of sources initially categorized as *Galaxies* were switched to *AGN* on the basis of their UV to near-IR colour. The specific requirement was for  $NUV - J < 5$ , where *NUV* is the near-UV magnitude from *GALEX* and the *J* magnitude is from the *2MASS*. The 18 objects that met this criterion are classed as *UVX* sources both in Table 3 and Table A.1.

Of the 219 *AGN* and galaxies comprising the XSS extragalactic sample, 181 have spectroscopic or photometrically estimated redshifts (see Table A.1). The distribution of redshifts is shown in Fig. 6. The mode of the distribution is at  $z \approx 0.05$ ; for a source at the survey limit the corresponding X-ray luminosity (for  $H_0 = 70 \text{ km s}^{-1} \text{ Mpc}^{-1}$ ) is  $\sim 1.7 \times 10^{43} \text{ erg s}^{-1}$  (2–10 keV).

### 4.2. Infrared colours

We have investigated the mid-IR and near-IR colours of the *AGN* and galaxies in the XSS extragalactic sample by utilising the WISE 3.4, 4.6, 12 and 22  $\mu\text{m}$  data (*i.e.*, the W1, W2, W3 and W4 bands respectively), and the *2MASS* J, H and K bands. Mid-IR and near-IR two-colour diagrams are shown in Fig. 7. These

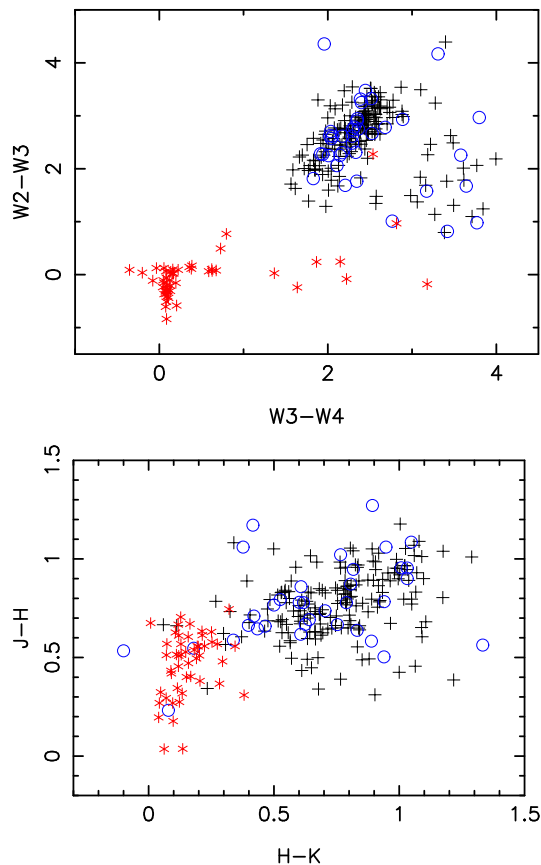


**Fig. 7.** The mid- and near-IR colours of the AGN and galaxies in the XSS extragalactic sample. *Top panel:* WISE W2-W3 versus W3-W4 two-colour diagram. *Bottom panel:* 2MASS J-H versus H-K two-colour diagram. In both cases, the XSS AGN are shown as crosses (black) and the galaxies as circles (blue). For comparison, the XSS sources categorized as stars are shown as asterisks (red).

diagrams demonstrate that the AGN and galaxies are well separated from the stellar coronal sources in terms of their W2-W3 colour (apart from one or two early type stars found in local star formation regions). With slightly less efficiency, the H-K colour also serves to distinguish between the extragalactic and Galactic X-ray source populations. We note that the sources in the XSS extragalactic sample occupy largely the same region of the mid-IR two-colour diagram as the luminous AGN in the Bright Ultra-Hard *XMM-Newton* Survey (Mateos et al. 2012).

#### 4.3. Cross-correlation with the SWIFT BAT catalogue

We have also investigated the coincidence of the XSS extragalactic sample with sources discovered in the hard (14–195 keV) X-ray band by the BAT experiment on Swift. For this purpose we use the on-line<sup>11</sup> Swift BAT 58-Month Hard X-ray Survey (Baumgartner et al. 2010). Using a 1′ search radius, there were 37 XSS-BAT matches, 6 of which were with XSS hard-only sources. Fig. 8 shows the correlation diagram for the 14–195 keV versus 2–10 keV fluxes, in which diagonal dotted lines delineate 14–195 keV:2–10 keV flux ratios of 1:1 and 10:1. For comparison, the lower ratio applies to a source exhibiting relatively soft

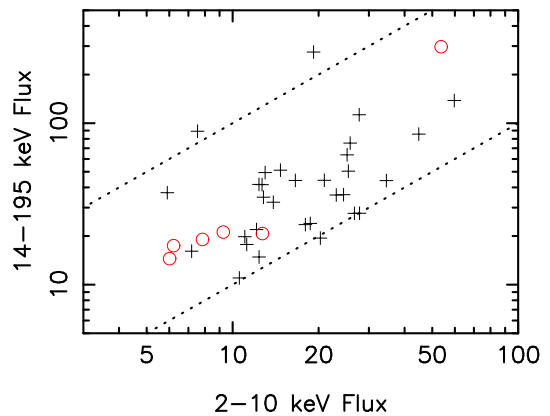


**Fig. 8.** The correlation between the 14–195 keV flux ( $10^{-12}$  erg  $\text{cm}^{-2}$   $\text{s}^{-1}$ ) measured by the BAT experiment on Swift and the XSS 2–10 keV flux ( $10^{-12}$  erg  $\text{cm}^{-2}$   $\text{s}^{-1}$ ) for the 37 cross matches. XSS hard+soft are shown as crosses, whereas XSS hard-only sources are shown as circles (red). The dotted lines represent BAT:XSS flux ratios of 1:1 and 10:1 respectively.

continuum emission ( $\Gamma \sim 2$ ) subject to a modest level of absorption ( $N_H \approx 10^{21}$   $\text{cm}^{-2}$ ), whereas a requisite for the higher ratio is either a very hard continuum ( $\Gamma \sim 1.0$ ) or substantial line-of-sight absorption ( $N_H > 10^{23}$   $\text{cm}^{-2}$ ).

Interestingly there were no BAT detections of any of the XSS sources classed as *Unidentified*.

## 5. Determination of the XSS source counts

A major objective of this investigation was to establish the log  $N$  - log  $S$  relation for a sample of extragalactic sources selected in the hard 2–10 keV from the XSS and to compare the results with those reported from other surveys. Given the small numbers of clusters detected in the XSS, the focus is necessarily on the identified sample of AGN and galaxies.

### 5.1. The results from a Monte Carlo simulation

Given the wide range of factors which might influence the detection probability of *real* sources and, for those sources with positive detections, might deviate the measured count rate from the true value, we have carried out a Monte Carlo simulation of the survey process.

In brief, this involved adding simulated sources at random positions to the set of sky images created as part of the slew survey pipeline. For a simulated source of specified count rate, the number of net counts was calculated on the basis of the effective exposure and then randomised according to Poissonian statistics. These counts were then distributed about the assigned source position according to the appropriate point spread function. The source detection algorithm was then applied and the number of counts net of the background determined from which a *measured count rate* could be assigned. The simulated source was classed as a detection and considered further provided all the criteria applied in the actual XSS selection were met (*e.g.*, a minimum of 4 net counts). Repetition of this process then allowed a count rate probability distribution appropriate to the specified input rate to be determined. Finally a series of trials were conducted so as to cover a representative range of input count rate; each of these trials were based on 10000 simulated sources, ex-

<sup>11</sup> Available at <http://heasarc.nasa.gov/docs/swift/results/bs58mon/>.



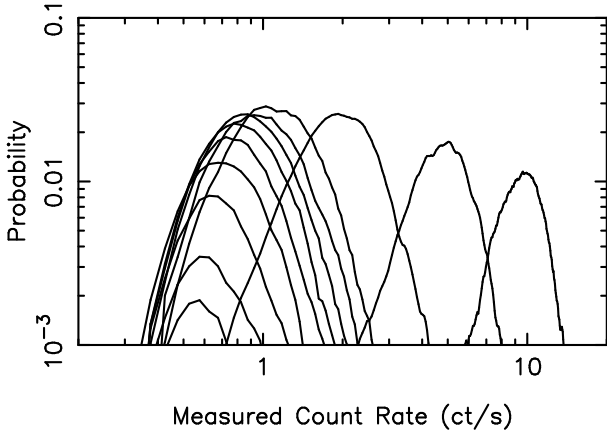


**Fig. 9.** Probability of measuring a given output count rate for simulated sources of fixed input count rate. These probability density functions are based on bins of 0.05 ct/s width and are smoothed versions of the raw simulation data (using a 1-d top-hat smoothing filter with a width of 5 bins). From left to right (based on the position of the peak) the curves correspond to input count rates of 0.1, 0.2, 0.3, 0.4, 0.5, 0.6, 0.7, 0.8, 1.0, 2.0, 5.0 and 10 ct/s. For this plot the normalisation of the 0.1 ct/s curve has been scaled upwards by a factor of 5.

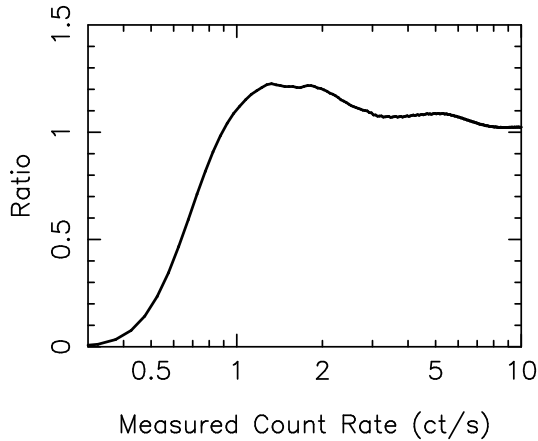


**Fig. 10.** Ratio of the predicted differential log N - log S function (as determined by the simulation) to the assumed input power-law form.

cept for the two trials at the lowest input count rates (0.1 and 0.2 ct/s) where 20000 sources were employed and the trial with the highest input rate (10 ct/s) which was based on 4000 sources.

Figure 9 shows the results of the simulation in the form of probability density curves plotted as a function of the measured count rate. The set of curves cover two decades of input count rate from 0.1 ct/s up to 10 ct/s. The detection probability evidently truncates at a measured count rate of  $\sim 0.4$  ct/s, *i.e.*, the 4 count threshold divided by the maximum exposure of  $\approx 10$  s. We note that even at very low input rates (*e.g.*, 0.2 ct/s for which the average count at maximum exposure is 2), there is still a finite probability that the source will be detected, since Poissonian deviations allow the occasional detection of the source at or above the 4 count threshold.

The next step was to use the curves in Fig. 9 to predict the number of sources detected as a function of the measured count rate. Here we took the underlying differential log N - log S function of the cosmic X-ray source population to be a powerlaw function with index  $\gamma$  and normalisation  $K$ :

$$N(S)dS = KS^{-\gamma}dS \quad (1)$$

where  $S$  is the true count rate in ct/s units and  $N(S)dS$  is the number of sources with true count rate in the range  $S$  to  $S + dS$ . We assumed  $\gamma = 2.5$  (*i.e.*, the Euclidean form of the source counts).

The range  $S = 0.1 - 20$  ct/s was divided into bins (of width 0.01 ct/s for  $S = 0.10-0.25$  ct/s and 0.1 ct/s thereafter) and the number of sources  $\Delta N$  within the bin calculated. For each value of  $S$  the corresponding probability density  $P(S_m)$  as a function of the measured count rate,  $S_m$  was determined, where necessary by interpolating across the curves shown in Fig.9. The summation of the  $\Delta N \times P(S_m)$  products over the full range of  $S$  then allowed the differential source count as a function of the *measured count rate*,  $M(S_m)$ , to be determined.

The ratio  $M(S_m)/N(S_m)$  is then a prediction, based on the simulation, of how closely the measured source counts will track the input form. Figure 10 shows this ratio for the range of count rates encompassed by our XSS sample. The simulation demonstrates the onset of a cutoff below a measured count rate of 1 ct/s with a sharp truncation at  $\approx 0.4$  ct/s. The prediction of a slight excess of sources with measured count rates from 1–3 ct/s most likely stems from the effect of Eddington bias. This is the process by which, through Poissonian fluctuations, faint sources are boosted to higher levels more frequently than bright sources are suppressed, by virtue of the numerical superiority of the former.

Further evidence of the major impact of Eddington bias on the XSS is provided in Fig. 11 which shows the spread in the true (input) count rate for sources detected at a particular measured count rate. For example, a measured count rate of 0.5 ct/s can derive from sources with true count rate anywhere between 0.1–1 ct/s. Even for much brighter sources the underlying uncertainty in the true count rate (and hence the source flux) is surprisingly large.

## 5.2. Extragalactic log N - log S relation

We have determined the source counts of the set of sources which comprise our extragalactic sample. A technical issue arises in relation to how to deal with the overlap of the *XMM-Newton* slews which comprise the XSS. As noted earlier, this overlap results in some duplicate source detections in the primary XSS database, which we subsequently removed in building our hard-band selected sample. However, the source count calculation is greatly simplified if we ignore this overlapping coverage, but commensurately add back the duplicate detections. In practice this involved adding 17 duplication detections to the set of 219 sources which comprise our extragalactic sample.

The integral source counts were determined by giving each source a weight  $N(S_m)/M(S_m)$  (*i.e.*, the reciprocal of the function plotted in Fig. 10) and then summing these weights as a function of decreasing  $S_m$ . The result is shown in Fig. 12 in a normalised form, *i.e.*, the measured integral counts divided by the integral version of the fiducial Euclidean source count defined previously.

The integral log N - log S curve for the extragalactic sources follows the Euclidean form below 3.0 ct/s. The normalisation implies 100 sources brighter than 1 ct/s are detected in the

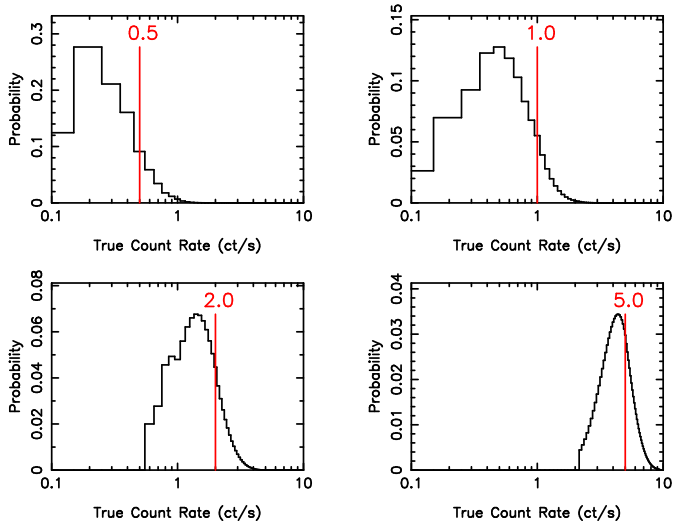


**Fig. 11.** Spread in the true (input) count rate for sources detected at different *measured* count rates. The four panels show the results for measured count rates of 0.5, 1.0, 2.0 and 5.0 ct/s (as represented by the vertical lines).

14233 square degree covered by the XSS (overlaps included), which, down to the limiting sensitivity of the XSS ( $0.4 \text{ ct/s} = 3.2 \times 10^{-12} \text{ erg cm}^{-2} \text{ s}^{-1}$ ) implies  $\sim 1000$  X-ray sources in the high-latitude sky above  $|b| > 10^\circ$  (excluding, of course, clusters of galaxies and Galactic objects). In Fig. 12 there is an apparent deficit of sources above 3.0 ct/s. In fact using the normalisation quoted above and assuming the Euclidean form for the counts extends from 3–10 ct/s, we predict 14 sources in this count rate range compared to the 9 sources in the actual sample. For a Poisson distribution, the chances of recording 9 or less events for a mean rate of 14 is 11%, implying that the deficit of bright sources in the XSS is not hugely significant.

By way of comparison, Fig. 12 also shows the integral counts for the 178 sources classed as *Unidentified* in the XSS hard-band selected sample. The steep form of this relation ( $\gamma \approx 3.0$ ) is difficult to match to any known astrophysical population and hence adds weight to the conjecture that most of these sources are spurious.

We have also derived the *differential* form of the log N - log S curve for the extragalactic sample. Figure 13 shows the result, again normalised to the Euclidean form. So as to make comparisons with other surveys, we have converted the XSS count rates to 2–10 keV fluxes using the conversion factor specified in §2.1. As noted above, within the flux range encompassed by the XSS, the counts of extragalactic objects (excluding clusters) follow the Euclidean form. Figure 13 also compares the XSS results with the differential 2–10 keV source counts at high latitude derived from the 2XMM catalogue (Mateos et al. 2008). The normalisation of the source counts at the high flux end of the 2XMM survey and at the low flux end of the XSS are very comparable, suggesting that a smooth interpolation is possible across the intervening gap (which amounts to a factor  $\sim 3$  in flux). There is, however, the caveat that the 2XMM data do not specifically exclude either Galactic interlopers or clusters of galaxies. Figure 13 also shows a point at high flux corresponding to the AGN sample defined by Piccinotti et al. (1982) on the basis of the

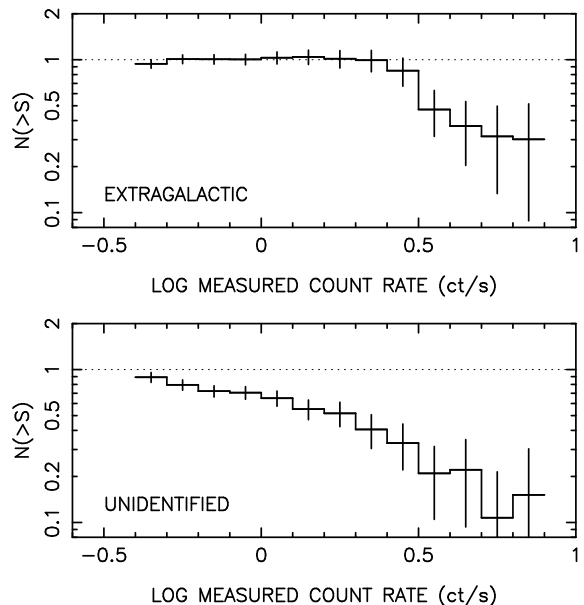


**Fig. 12.** *Top panel:* Integral log N - log S curve for the extragalactic XSS sample (excluding clusters of galaxies) normalised to  $N(>S) = 100 \times S^{-1.5}$ . *Bottom panel:* Integral log N - log S curve for the sources classed as *Unidentified* in the XSS hard-band selected sample.

*HEAO-1* A2 survey. Here the agreement with XSS is good, apart from the apparent deficit in the highest XSS bin<sup>12</sup>.

To aid the interpretation of the source counts we have also plotted in Fig. 13, the predictions of Gilli, Comastri & Hasinger (2007) for the 2–10 keV band both for AGN alone and for AGN plus clusters of galaxies. There is clearly excellent agreement between the AGN prediction and the measured XSS counts. In the flux range of the XSS, we might expect that the inclusion of clusters in the extragalactic sample would result in an additional 80%-100% of sources (consistent with the Piccinotti et al results where clusters represented half the total extragalactic sample). Clearly this reemphasises the point made earlier that there is a very strong selection bias against extended sources in the XSS catalogue. Figure 13 also provides at least a hint that some clusters of galaxies may also be missing from the 2XMM catalogue (Mateos et al. 2008).

## 6. Summary and Conclusions

The substantial sky coverage afforded by the XSS makes this survey a unique resource for studying X-ray bright source samples. We have shown that, with care, the XSS can be used to define reliable subsets of sources selected in the 2–10 keV band, down to a limiting sensitivity of  $3 \times 10^{-12} \text{ ergs cm}^{-2} \text{ s}^{-1}$  and encompassing sources with as few as 4 counts net of the background. One caveat is that there is a significant bias against the detection of extended sources, such as clusters of galaxies. A second caveat is that a significant fraction ( $\approx 75\%$ ) of the faint XSS sources detected solely in the hard band may in fact be spurious detections.

<sup>12</sup> In this case roughly 4 additional sources would be required in the highest flux bin (encompassing sources with count rates from 5-10 ct/s) so as to raise this bin to an ordinate value of 0.5.

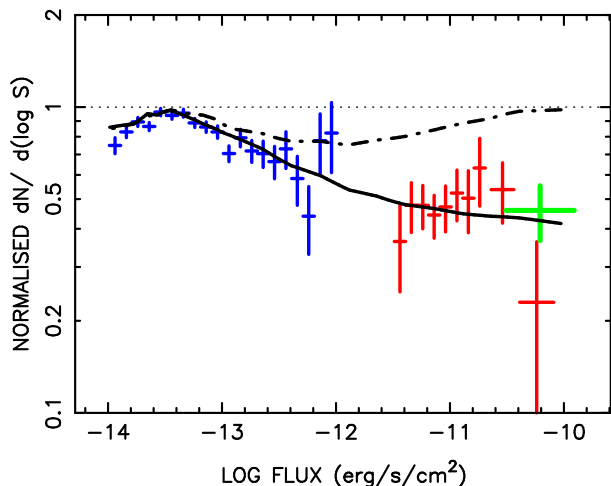


**Fig. 13.** Differential 2–10 keV log N - log S curve for the XSS extragalactic sample (red data points), normalised to the Euclidean form. At the faint end the XSS results are compared with the differential 2–10 keV source counts derived from the 2XMM catalogue by Mateos et al. (2008) (blue points). At the bright end the comparison is with the *HEAO-1* A2 AGN sample of Piccinotti et al. (1982) (green point). The solid curve is the prediction of the AGN source counts from the work of Gilli, Comastri & Hasinger (2007). The dot-dashed curve similarly represents the prediction of the total extragalactic counts, *i.e.*, AGN plus clusters of galaxies. In drawing these comparisons account has been taken of the relevant survey sky areas. In this plot the normalisation factor has been matched to the counts of the AGN plus clusters at the high flux end.

For the purpose of source identification, the XSS is well matched to currently available all-sky IR surveys such as 2MASS and WISE. For the XSS sources detected simultaneously in the XSS hard and soft bands, the hit rate with WISE was close to 100%, in the case of the AGN/galaxies and stellar coronal emitters. The infrared colours of the counterparts also provides a rather efficient method of removing the active stars when constructing an extragalactic sample. Unfortunately, for the XSS sources detected only in the hard band, the search for WISE counterparts is somewhat compromised by the high chance rate that applies when the sample size is inflated by spurious detections.

A major motivation of this work was to use the XSS to determine the extragalactic log N - log S relation in a flux regime which is poorly sampled by existing surveys. To that end we constructed an XSS extragalactic sample comprised of 219 sources with likely identifications as AGN/galaxies, but necessarily excluding clusters of galaxies. Using the results of a detailed simulation of the source detection procedure we were able to apply corrections for the complex selection biases which come into play in the low-count regime of the XSS. The conclusion of this study was that the normalisation we derive for the XSS extragalactic source counts fits well with published measurements at brighter and fainter levels, which together span 4 decades in X-ray flux.

*Acknowledgements.* AMR acknowledges STFC/UKSA funding support. We thank Silvia Mateos for providing the 2XMM source count data in a convenient form. This research has made use of the SIMBAD and Vizier facilities at CDS, Strasbourg and the NASA/IPAC Extragalactic Database (NED). This publication utilises data from the Two Micron All Sky Survey, which is a joint project of the

University of Massachusetts and IPAC/Caltech. This paper has also made use of the source catalogue from the Wide-field Infrared Survey Explorer, which is a NASA sponsored joint project of the University of California, Los Angeles, and the Jet Propulsion Laboratory/California Institute of Technology. Use was also made of data from the Galaxy Evolution Explorer, GALEX, which is operated for NASA by the California Institute of Technology under NASA contract NAS5-98034. The XMM-Newton project is an ESA science mission with instruments and contributions directly funded by ESA member states and the USA (NASA).

## References

- Alexander, D.M., Bauer, F.E., Brandt, W.N., et al., AJ, 126, 539  
 Baumgartner, W.H., Tueller, J., Markwardt, C., Skinner, G., 2010, BAAS, 41, 675  
 Brunner, H., Cappelluti, N., Hasinger, G.; Barcons, X., Fabian, A. C., Mainieri, V., Szokoly, G., 2008, A&A, 479, 283  
 Comastri, A., Ranalli, P., Iwasawa, K., Vignali, C., Gilli, R., Georgantopoulos, I., Barcons, X., Brandt, W.N., Brunner, H., Brusa, M., et al., 2011, A&A, 526, 9  
 Cutri, R. M., et al. 2003, Explanatory Supplement to the 2MASS All-Sky Data Release and Extended Mission Products (Pasadena:IPAC/Caltech)  
 Cutri, R. M., et al. 2012, Explanatory Supplement to the WISE All-Sky Data Release Products (Pasadena:IPAC/Caltech)  
 Elvis, M., Civano, F., Vignali, C., Puccetti, S., Fiore, F., Cappelluti, N., Aldcroft, T. L., Fruscione, A., Zamorani, G., Comastri, A., et al., 2009, ApJS, 184, 158  
 Forman, W., Jones, C., Julien, P., Murray, S., Peters, G., Tananbaum, H., Giacconi, R., 1978, ApJS, 38, 357  
 Gilli, R., Comastri, A., Hasinger, G., 2007, A&A, 463, 79  
 Giommi, P., Perri, M., Fiore, F., 2000, A&A, 362, 799  
 Luo, B., Bauer, F. E., Brandt, W. N., Alexander, D. M., Lehmer, B. D., Schneider, D. P., Brusa, M., Comastri, A., Fabian, A. C., Finoguenov, A., et al., 2008, ApJS, 179, 19  
 Martin, D.C., Fanson, J., Schiminovich, D., et al. 2005, ApJ, 619, L1  
 Mateos, S., Warwick, R. S., Carrera, F. J., Stewart, G. C., Ebrero, J., Della Ceca, R., Caccianiga, A., Gilli, R., Page, M. J., Treister, E., Tedds, J. A., Watson, M. G., Lamer, G., Saxton, R. D., Brunner, H., Page, C. G., 2008, A&A, 492, 51  
 Mateos, S., Alonso-Herro, A., Carrera, F.J., Blain, A., Watson, M.G., Barcons, X., Braitto, V., Severgnini, P., Donley, J.L., 2012, MNRAS, in press  
 McHardy, I. M., Lawrence, A., Pye, J. P., Pounds, K. A., 1981, MNRAS, 197, 893  
 Piccinotti, G., Mushotzky, R. F., Boldt, E. A., Holt, S. S., Marshall, F. E., Serlemitsos, P. J., Shafer, R. A., 1982, ApJ, 253, 485  
 Saxton, R.D., Read, A.M., Esquej M.P., Freyberg M.J., Altieri, B., Bermejo, D., 2008, A&A, 480, 611  
 Saxton, R.D., Gimeno, C.D-T., 2011, ASPC, 442, 567  
 Skrutskie, M. F., Cutri, R. M., Stiening, R., Weinberg, M. D., Schneider, S., Carpenter, J. M., Beichman, C., Capps, R., Chester, T., Elias, J., et al., 2006, AJ, 131, 1163  
 Starling, R.L.C., Evans, P.A., Read, A.M., Saxton, R.D., Esquej, P., Krimm, H., O'Brien, P.T., Osborne, J.P., Mateos, S., Warwick, R., Wiersema, K., 2011, MNRAS, 412, 1853  
 Ueda, Y., Ishisaki, Y., Takahashi, T., Makishima, K., Ohashi, T., 2005, ApJS, 161, 185  
 Voges, W., Aschenbach, B., Boller, T., Braeuninger, H., Burkert, W., Dennerl, K., Englhauser, J., Gruber, R., Haberl, F., et al., 1999, A&A, 349, 389  
 Warwick, R. S., Pérez-Ramírez, D., Byckling, K., 2011, MNRAS, 413, 595  
 Watson, M. G., Schröder, A. C., Fyfe, D., Page, C. G., Lamer, G., Mateos, S., Pye, J., Sakano, M., Rosen, S., Ballet, J., et al., 2009, A&A, 493, 339  
 Wood, K. S., Meekins, J. F., Yentis, D. J., Smathers, H. W., McNutt, D. P., Bleach, R. D., Friedman, H., Byram, E. T., Chubb, T. A., Meidav, M., 1984, ApJS, 56, 507  
 Xue, Y. Q., Luo, B., Brandt, W. N., Bauer, F. E., Lehmer, B. D., Broos, P. S., Schneider, D. P., Alexander, D. M., Brusa, M., Comastri, A., et al., 2011, ApJS, 195, 10

**Appendix A:**

Details of the sources which comprise the hard-band selected XSS extragalactic sample - see Table A.1. The table provides the following information for each source: the XSS name; whether the source was also detected in the XSS soft band; the XSS hard band (2–10 keV) flux and error on the flux (in units of  $10^{-11}$  ergs  $\text{cm}^{-2}$   $\text{s}^{-1}$ ); the RA and Dec of the proposed counterpart; the name of the counterpart; the type of the counterpart; the redshift (if known). The table is available as a FITS file from the authors.

**Table A.1.** Sources comprising the XSS extragalactic sample

Slew ID	Soft	Flux	RA	Dec	ID	Type	Redshift
XMMSL1 J000226.3+032108	Y	0.64±0.22	0.6101	3.3520	NGC 7811	Sy1	0.025
XMMSL1 J001439.7+183449	-	0.56±0.18	3.6671	18.5822	NGC 52	Gal	0.018
XMMSL1 J003621.2+453958	Y	0.72±0.21	9.0873	45.6649	Zw 535.012	Sy1.2	0.047
XMMSL1 J004146.6-470141	Y	0.77±0.19	10.4459	-47.0269	RBS 97	BLLac	0.15
XMMSL1 J004755.6+394907	Y	0.56±0.21	11.9801	39.8160	5C 3.178	BLLac	0.252
XMMSL1 J004819.1+394119	Y	0.42±0.20	12.0791	39.6866	B0045+3926	Sy1	0.134
XMMSL1 J005953.1+314934	Y	1.43±0.32	14.9720	31.8270	Mrk 0352	Sy1	0.014
XMMSL1 J010512.2+802712	Y	0.60±0.17	16.2970	80.4520	WISE J010511.28+802707.2	Gal	-
XMMSL1 J011209.0+330310	Y	0.45±0.21	18.0400	33.0538	GALEX J011209.5+330313	UVX	0.159
XMMSL1 J011423.7-552358	-	0.78±0.24	18.6039	-55.3970	NGC 454E	Sy2	0.012
XMMSL1 J012345.1-584822	Y	2.54±0.65	20.9407	-58.8058	FAIRALL 9	Sy1	0.047
XMMSL1 J012950.7-421934	-	1.68±0.52	22.4631	-42.3265	ESO 244-30	QSO	0.025
XMMSL1 J015025.1+091453	Y	0.55±0.20	27.6056	9.2476	PHL 1186	Sy1.5	0.27
XMMSL1 J015251.0-523830	Y	0.42±0.19	28.2149	-52.6401	GALEX J015251.3-523826	UVX	0.077
XMMSL1 J020124.1+021545	-	0.91±0.39	30.3518	2.2643	WISE J020124.44+021551.3	Gal	0.085
XMMSL1 J020306.6-385423	Y	0.49±0.18	30.7782	-38.9065	PGC 109903	RG	0.144
XMMSL1 J020615.7-001731	Y	1.39±0.36	31.5666	-0.2914	Mrk 1018	Sy1.5	0.042
XMMSL1 J020921.4-522922	Y	2.11±0.53	32.3400	-52.4897	RBS 0285	BLLac	-
XMMSL1 J021734.8-725126	Y	0.91±0.25	34.3986	-72.8578	SUMSS J021735-725125	UVX	0.29
XMMSL1 J022625.4-282054	Y	0.73±0.26	36.6071	-28.3497	HE 0224-2834	Sy1	0.06
XMMSL1 J023005.6-085950	Y	1.34±0.38	37.5230	-8.9981	Mrk 1044	Sy1	0.016
XMMSL1 J023248.4+201720	Y	1.49±0.33	38.2025	20.2881	BWE 0229+2004	BLLac	0.14
XMMSL1 J023819.5-521129	Y	1.90±0.42	39.5821	-52.1923	ESO 198-24	Sy1	0.045
XMMSL1 J030315.6-121326	Y	0.80±0.21	45.8149	-12.2249	PGC 955931	RG	0.077
XMMSL1 J031028.1-004950	Y	0.37±0.15	47.6159	-0.8307	LBQS 0307-0101	Sy1	0.08
XMMSL1 J031118.7-204618	Y	2.78±0.63	47.8284	-20.7717	HE 0309-2057	Sy1	0.066
XMMSL1 J035141.4-402758	Y	1.06±0.31	57.9237	-40.4665	FAIRALL 1116	Sy1	0.058
XMMSL1 J035257.3-683117	Y	3.62±0.64	58.2395	-68.5214	PKS 0352-686	RG	0.087
XMMSL1 J035324.7-404927	-	0.82±0.35	58.3533	-40.8265	WISE J035324.78-404935.2	Gal	-
XMMSL1 J041241.2-471252	Y	0.54±0.17	63.1728	-47.2128	RBS 518	Sy1	0.132
XMMSL1 J041959.8-545618	Y	1.25±0.43	65.0016	-54.9380	NGC 1566	Sy1.5	0.0050
XMMSL1 J042224.4-561333	-	0.51±0.20	65.6002	-56.2256	ESO 157-23	Sy2	0.043
XMMSL1 J042559.7-571142	Y	1.80±0.30	66.5030	-57.2005	1H0419-577	Sy1	0.104
XMMSL1 J043429.6+712747	Y	0.45±0.16	68.6213	71.4672	IRAS 04288+7121	Sy1	0.024
XMMSL1 J043958.6-594049	-	0.77±0.24	69.9960	-59.6816	ESO 118-33	Sy2	0.057
XMMSL1 J044347.0+285822	Y	1.30±0.47	70.9450	28.9719	UGC 3142	Sy1	0.021
XMMSL1 J045003.8+260016	-	0.91±0.41	72.5175	26.0049	WISE J045004.20+260017.7	Gal	0.373
XMMSL1 J045014.5-142557	-	0.40±0.15	72.5618	-14.4326	IRAS 04479-1431	Gal	0.038
XMMSL1 J050432.4-734925	-	0.69±0.20	76.1428	-73.8243	WISE J050434.26-734927.2	Gal	0.045
XMMSL1 J050956.9-641741	Y	0.74±0.23	77.4886	-64.2949	GALEX J050957.2-641742	QSO	-
XMMSL1 J051622.4+192701	-	1.27±0.31	79.0946	19.4531	IRAS 05134+1923	Gal	0.021
XMMSL1 J051949.5-454642	Y	0.59±0.20	79.9572	-45.7789	PICTOR A	Sy1	0.035
XMMSL1 J053756.2-024516	Y	0.76±0.28	84.4846	-2.7536	WISE J053756.30-024513.1	Gal	0.58
XMMSL1 J054357.2-553208	Y	0.81±0.22	85.9884	-55.5354	RBS 679	BLLac	-
XMMSL1 J054641.6-641518	Y	1.20±0.35	86.6743	-64.2561	GALEX J054641.8-641521	Sy1	0.323
XMMSL1 J055040.6-321617	Y	2.67±0.44	87.6690	-32.2713	B0548-322	QSO	0.069
XMMSL1 J055211.9-072723	-	5.37±0.89	88.0474	-7.4562	NGC 2110	Sy2	0.0078
XMMSL1 J060649.6-624547	Y	0.67±0.24	91.7070	-62.7622	GALEX J060649.6-624543	UVX	-
XMMSL1 J061100.0-491036	Y	0.49±0.18	92.7507	-49.1763	GALEX J061100.1-491033	QSO	-
XMMSL1 J062706.2-352916	Y	1.22±0.29	96.7780	-35.4876	PKS 0625-354	LINER	0.054
XMMSL1 J063326.2-561416	-	0.59±0.20	98.3609	-56.2392	WISE J063326.61-561420.9	Gal	0.047
XMMSL1 J063957.2+384840	Y	0.80±0.22	99.9894	38.8107	B0636+3851	QSO	-
XMMSL1 J071030.7+590807	Y	2.03±0.42	107.6253	59.1390	B0706+5913	BLLac	0.125
XMMSL1 J072927.7+243622	Y	0.60±0.22	112.3659	24.6066	B2 0726+24	Sy2	0.163
XMMSL1 J072956.7-654338	Y	0.61±0.27	112.4878	-65.7258	6dFGS g0729571-654333	UVX	0.08
XMMSL1 J073956.1+280151	-	1.77±0.51	114.9844	28.0290	GALEX J073956.2+280145	UVX	0.081
XMMSL1 J074021.7-581544	-	0.40±0.16	115.0934	-58.2634	WISE J074022.41-581548.2	Gal	-
XMMSL1 J074126.3+354716	Y	0.78±0.19	115.3599	35.7841	GALEX J074126.3+354702	QSO	-
XMMSL1 J075051.9+123101	Y	0.46±0.18	117.7169	12.5180	B0748+126	QSO	0.889
XMMSL1 J075118.9-665728	-	0.49±0.17	117.8269	-66.9578	WISE J075118.44-665727.9	Gal	-
XMMSL1 J075244.5+455655	Y	0.68±0.20	118.1842	45.9493	NPM1G+46.0092	Sy1.9	0.051
XMMSL1 J080157.9-494648	Y	1.21±0.40	120.4915	-49.7785	ESO 209-12	Sy1	0.04
XMMSL1 J080327.6+084156	Y	1.67±0.29	120.8641	8.6979	FIRST J080327.4+084152	Gal	0.047
XMMSL1 J081917.6-075626	Y	1.21±0.44	124.8233	-7.9406	RX J0819.2-0756	BLLac	-
XMMSL1 J083014.8-094505	Y	0.86±0.21	127.5631	-9.7488	GALEX J083015.1-094456	QSO	-

Table A.1. Continued

Slew ID	Soft	Flux	RA	Dec	ID	Type	Redshift
XMMSL1 J083015.3-672527	Y	0.67±0.17	127.5690	-67.4248	GALEX J083016.5-672528	UVX	0.035
XMMSL1 J083950.7-121434	Y	0.76±0.27	129.9608	-12.2429	PKS 0837-12	Sy1.2	0.197
XMMSL1 J084314.1+535706	Y	0.61±0.24	130.8059	53.9553	SBS 0839+541	Sy1	0.218
XMMSL1 J085036.8+044354	Y	0.88±0.32	132.6548	4.7326	GALEX J085037.1+044356	QSO	-
XMMSL1 J085454.2-242337	Y	1.14±0.34	133.7299	-24.3937	GALEX J085455.1-242337	UVX	0.091
XMMSL1 J085841.0+104134	-	0.45±0.17	134.6740	10.6895	IRAS 08559+1053	Sy2	0.149
XMMSL1 J090816.9+052012	Y	0.51±0.20	137.0715	5.3338	SDSS J090816.78+052012.0	QSO	0.344
XMMSL1 J090822.3-643749	Y	1.39±0.34	137.0937	-64.6311	WISE J090822.49-643751.7	Gal	-
XMMSL1 J091300.4-210324	Y	2.24±0.51	138.2509	-21.0559	6dFGS gJ091300.2-210321	BLLac	0.198
XMMSL1 J092342.9+225435	Y	1.24±0.35	140.9292	22.9091	CGCG 121-075	Sy1.2	0.032
XMMSL1 J092616.5-842131	-	0.71±0.23	141.5740	-84.3594	IRAS 09305-8408	Sy2	0.062
XMMSL1 J093909.6-211252	Y	0.50±0.18	144.7907	-21.2141	GALEX J093909.7-211250	QSO	-
XMMSL1 J094745.3+072521	-	0.38±0.15	146.9381	7.4224	3C 227	Sy1	0.087
XMMSL1 J095303.0-765802	Y	0.70±0.25	148.2683	-76.9673	SUMSS J095303-765804	Gal	-
XMMSL1 J095534.3+690350	Y	1.24±0.32	148.8883	69.0654	M 81	LINER	1.4E-4
XMMSL1 J095942.7-311255	Y	1.12±0.26	149.9277	-31.2162	1RXS J095942.1-311300	Sy1	0.037
XMMSL1 J100207.0+030333	Y	0.64±0.16	150.5293	3.0577	IC 588	QSO	0.023
XMMSL1 J100955.8+261129	-	0.96±0.32	152.4848	26.1922	GALEX J100956.1+261132	UVX	0.241
XMMSL1 J102330.4+195157	Y	2.77±0.41	155.8774	19.8651	NGC 3227	Sy1.5	0.0039
XMMSL1 J102356.0-433610	Y	1.45±0.27	155.9842	-43.6004	RXS J10239-4336	BLLac	-
XMMSL1 J104833.4-390244	Y	1.02±0.31	162.1410	-39.0439	GALEX J104833.8-390237	UVX	0.044
XMMSL1 J105639.8-312213	Y	0.41±0.17	164.1659	-31.3700	GALEX J105639.8-312211	QSO	-
XMMSL1 J110427.8+381230	Y	5.97±0.73	166.1139	38.2089	Mrk 421	BLLac	0.03
XMMSL1 J112048.4+421212	Y	1.39±0.46	170.2003	42.2035	BWE 1118+4228	BLLac	0.124
XMMSL1 J112654.2+185007	-	0.35±0.15	171.7295	18.8326	MCG +03-29-049	RG	0.019
XMMSL1 J112715.8+190917	Y	1.32±0.27	171.8180	19.1556	1RXS J112716.6+190914	Sy1	0.1
XMMSL1 J112736.7+244918	Y	0.76±0.25	171.9038	24.8232	GALEX J112736.9+244924	QSO	0.059
XMMSL1 J112841.5+575017	Y	0.35±0.14	172.1709	57.8352	MCG +10-17-004	Sy2	0.051
XMMSL1 J113104.0+685156	Y	0.92±0.49	172.7699	68.8647	EXO 1128.1+6908	Sy1	0.043
XMMSL1 J113626.2+700926	Y	1.43±0.41	174.1101	70.1575	B1136+704	BLLac	0.045
XMMSL1 J120058.3+064828	-	0.93±0.29	180.2415	6.8064	WISE J120057.95+064823.0	Gal	0.036
XMMSL1 J121044.4+382010	-	0.50±0.19	182.6845	38.3362	KUG 1208+386	Sy1	0.023
XMMSL1 J121158.5+224235	Y	0.67±0.25	182.9943	22.7092	FIRST J121158.6+224232	BLLac	0.455
XMMSL1 J121749.9+354454	Y	0.44±0.19	184.4575	35.7471	GALEX J121749.7+354448	UVX	0.088
XMMSL1 J121826.6+294846	Y	1.24±0.31	184.6105	29.8130	Mrk 766	Sy1	0.012
XMMSL1 J122121.9+301040	Y	1.38±0.45	185.3415	30.1770	B1218+304	BLLac	0.182
XMMSL1 J122324.3+024052	Y	1.87±0.37	185.8506	2.6791	Mrk 50	Sy1.2	0.023
XMMSL1 J122546.2+123930	Y	1.92±0.40	186.4449	12.6622	NGC 4388	Sy2	0.0084
XMMSL1 J123135.7+704413	Y	0.50±0.18	187.9024	70.7374	RX J1231.6+7044	Sy1	0.208
XMMSL1 J123203.4+200930	Y	1.24±0.33	188.0151	20.1582	Mrk 771	Sy1	0.063
XMMSL1 J125212.3-132455	Y	1.44±0.42	193.0520	-13.4147	NGC 4748	Sy1	0.014
XMMSL1 J125341.2-393156	Y	0.74±0.19	193.4219	-39.5332	SHBL J125341.1-393159	QSO	0.19
XMMSL1 J125456.5-265704	Y	0.76±0.19	193.7348	-26.9505	AM 1252-264	Sy1	0.059
XMMSL1 J125611.0-054720	Y	1.28±0.35	194.0466	-5.7893	3C 279	QSO	0.536
XMMSL1 J125616.0-114632	Y	0.81±0.27	194.0665	-11.7770	6dFGS g1256160-114637	Gal	0.058
XMMSL1 J125657.1-095017	-	1.22±0.46	194.2370	-9.8374	HE 1254-0934	Sy1	0.139
XMMSL1 J130258.9+162427	Y	1.32±0.35	195.7452	16.4077	Mrk 783	Sy1	0.067
XMMSL1 J130323.0-134132	Y	0.45±0.19	195.8427	-13.6925	NPM1G-13.0407	Sy1.2	0.046
XMMSL1 J130359.4+033932	-	0.51±0.22	195.9978	3.6590	FIRST J130359.5+033932	Sy1	0.184
XMMSL1 J130708.7+342417	Y	0.59±0.21	196.7866	34.4061	Mrk 64	Sy1.2	0.185
XMMSL1 J131305.8-110745	Y	0.92±0.24	198.2741	-11.1284	II SZ 10	Sy1.5	0.034
XMMSL1 J131424.0+271919	Y	0.74±0.24	198.5981	27.3222	CASG 991	Sy1	0.133
XMMSL1 J131516.5+442427	-	0.79±0.30	198.8222	44.4072	UGC 8327	QSO	0.036
XMMSL1 J133239.1-102853	Y	0.64±0.22	203.1630	-10.4812	MCG -02-35-001	Sy1	0.022
XMMSL1 J133553.1-341745	Y	2.52±0.49	203.9741	-34.2956	MCG -06-30-015	Sy1.5	0.0070
XMMSL1 J133718.8+242258	Y	0.50±0.17	204.3280	24.3843	B1334+2438	Sy1	0.107
XMMSL1 J133844.1+242945	-	1.03±0.41	204.6814	24.5009	WISE J133843.54+243003.0	QSO	0.055
XMMSL1 J134105.2+395946	Y	0.88±0.20	205.2713	39.9960	7C 1338+4015	BLLac	0.163
XMMSL1 J134356.6+253849	Y	0.60±0.27	205.9865	25.6466	B1341+258	Sy1	0.087
XMMSL1 J134442.0-451002	-	0.79±0.29	206.1741	-45.1687	PGC 529701	Gal	0.145
XMMSL1 J134519.4+414243	Y	0.97±0.28	206.3299	41.7124	NGC 5290	QSO	0.0085
XMMSL1 J134915.2+220029	Y	0.49±0.19	207.3134	22.0091	IRAS F13469+2215	Sy1	0.062
XMMSL1 J135304.2+691826	Y	1.66±0.52	208.2644	69.3082	B1351+695	Sy1	0.03
XMMSL1 J140743.6-430516	Y	1.27±0.31	211.9323	-43.0858	WISE J140743.75-430508.8	Gal	-
XMMSL1 J140806.7-302348	Y	0.49±0.18	212.0283	-30.3983	EQ 1405-301	Sy1	0.023

Table A.1. Continued

Slew ID	Soft	Flux	RA	Dec	ID	Type	Redshift
XMMSL1 J141117.1-340323	Y	0.69±0.29	212.8238	-34.0560	6dFGS g1411177-340321	UVX	0.037
XMMSL1 J141922.4-263841	Y	3.46±0.56	214.8434	-26.6447	ESO 511-030	Sy1	0.022
XMMSL1 J142129.5+474724	Y	0.72±0.25	215.3740	47.7902	SBS 1419+480	Sy1.5	0.072
XMMSL1 J142149.3-380901	Y	0.94±0.29	215.4628	-38.1483	WISE J142151.07-380853.7	Gal	-
XMMSL1 J142239.3+580156	Y	1.17±0.31	215.6620	58.0321	QSO B1422+580	BLLac	0.634
XMMSL1 J143342.1-730442	Y	0.76±0.20	218.4286	-73.0772	GALEX J143343.0-730437	QSO	-
XMMSL1 J144923.5-063835	Y	0.86±0.30	222.3472	-6.6471	PGC 1030451	Gal	0.085
XMMSL1 J144932.5+274624	Y	0.89±0.27	222.3862	27.7728	RBS 1434	BLLac	0.225
XMMSL1 J145108.6+270928	Y	0.94±0.38	222.7866	27.1575	QSO B1448+273	Sy1	0.065
XMMSL1 J145307.4+255432	Y	2.10±0.38	223.2830	25.9092	GALEX J145307.9+255433	QSO	0.048
XMMSL1 J145907.4+714011	-	1.01±0.29	224.7817	71.6722	3C 309.1	Sy1	0.905
XMMSL1 J150401.2+102618	Y	2.45±0.75	226.0050	10.4378	Mrk 841	Sy1.5	0.036
XMMSL1 J150745.4+512716	-	0.66±0.28	226.9375	51.4529	Mrk 845	Sy1	0.046
XMMSL1 J151618.8-152345	Y	0.35±0.16	229.0780	-15.3956	1RXS J151618.7-152347	BLLac	-
XMMSL1 J153500.6+532035	Y	0.77±0.22	233.7534	53.3437	B1533+535	BLLac	0.89
XMMSL1 J153552.4+575415	Y	1.39±0.29	233.9684	57.9027	Mrk 290	Sy1	0.029
XMMSL1 J154016.3+815507	Y	1.93±0.54	235.0663	81.9182	1ES 1544+820	BLLac	0.271
XMMSL1 J154631.4-282217	Y	0.55±0.21	236.6306	-28.3695	GALEX J154631.3-282210	RG	0.121
XMMSL1 J154815.8+694942	Y	0.56±0.24	237.0697	69.8265	RX J1548.3+6949	QSO	0.375
XMMSL1 J154824.8-134526	Y	1.27±0.26	237.1040	-13.7576	NGC 5995	Sy1.9	0.025
XMMSL1 J155542.9+111126	Y	2.38±0.51	238.9294	11.1901	PG 1553+11	BLLac	0.36
XMMSL1 J161124.7+585102	Y	0.52±0.15	242.8529	58.8504	SBS 1610+589	Sy1.5	0.032
XMMSL1 J161126.8+724027	-	0.51±0.23	242.8624	72.6745	WISE J161126.98+724028.1	Gal	-
XMMSL1 J161658.4+643845	Y	0.45±0.19	244.2428	64.6450	HS 1616+6445	Sy1	0.171
XMMSL1 J161752.8-771723	Y	0.56±0.23	244.4628	-77.2929	QSO B1610-771	QSO	1.71
XMMSL1 J162532.1+852949	Y	0.91±0.29	246.3583	85.4949	VII Zw 653	Sy1.2	0.063
XMMSL1 J162948.1+672245	Y	0.71±0.32	247.4516	67.3784	Mrk 0885	Sy1.5	0.052
XMMSL1 J164734.8+495013	Y	0.53±0.19	251.8944	49.8387	RXS J16475+4950	Sy1	0.047
XMMSL1 J165218.8+555415	-	0.60±0.17	253.0787	55.9056	UGC 10593	Sy2	0.029
XMMSL1 J170025.5-724045	Y	0.57±0.21	255.1059	-72.6791	GALEX J170025.1-724044	UVX	0.104
XMMSL1 J170330.6+454041	Y	0.49±0.16	255.8766	45.6798	B3 1702+457	Sy1	0.061
XMMSL1 J170500.6-013227	Y	0.93±0.34	256.2516	-1.5413	UGC 10683	Sy1	0.03
XMMSL1 J172504.4+115213	Y	1.39±0.35	261.2681	11.8710	QSO B1722+119	BLLac	0.018
XMMSL1 J172700.3+181422	Y	0.55±0.17	261.7535	18.2390	GALEX J172700.7+181420	QSO	-
XMMSL1 J173336.0+363130	-	0.91±0.33	263.4037	36.5255	WISE J173336.88+363131.8	Gal	-
XMMSL1 J174037.2+521139	Y	0.50±0.19	265.1541	52.1954	QSO B1739+522	QSO	1.375
XMMSL1 J174209.3+510107	Y	0.66±0.28	265.5385	51.0181	GALEX J174209.2+510105	UVX	0.063
XMMSL1 J174357.7+193511	Y	1.93±0.37	265.9910	19.5859	B1741+196	BLLac	0.083
XMMSL1 J174415.0+325930	Y	1.13±0.32	266.0603	32.9915	87 GB174224.8+3300	Gal	0.076
XMMSL1 J174508.2+015448	-	0.45±0.21	266.2826	1.9118	WISE J174507.82+015442.5	Gal	-
XMMSL1 J174538.1+290820	Y	1.10±0.31	266.4095	29.1395	GALEX J174538.2+290822	Sy1	0.111
XMMSL1 J175104.6+744742	Y	0.48±0.20	267.7701	74.7956	PGC 60979	Gal	0.025
XMMSL1 J180058.3+541035	Y	0.56±0.19	270.2436	54.1745	GALEX J180058.5+541027	UVX	-
XMMSL1 J180951.8-655615	-	0.70±0.21	272.4679	-65.9371	PMN J1809-6556	Gal	0.18
XMMSL1 J182021.1+362339	Y	0.42±0.16	275.0875	36.3953	GALEX J182021.0+362344	QSO	-
XMMSL1 J182609.9+545005	Y	0.94±0.29	276.5457	54.8349	WISE J182610.95+545005.7	Gal	-
XMMSL1 J183503.4+324143	Y	4.49±0.81	278.7641	32.6964	4C 32.55	Sy1	0.057
XMMSL1 J183658.3-592405	Y	2.09±0.50	279.2426	-59.4023	FRL 49	Sy2	0.02
XMMSL1 J185649.5-544233	Y	1.92±0.55	284.2057	-54.7083	6dFGS g1856494-544230	UVX	0.056
XMMSL1 J190939.2-622852	Y	1.89±0.42	287.4120	-62.4820	ESO 104-41	UVX	0.082
XMMSL1 J191028.2+495606	Y	0.44±0.16	287.6186	49.9348	WISE J191028.46+495605.4	Gal	0.146
XMMSL1 J191921.7+502646	Y	0.53±0.22	289.8421	50.4463	PGC 2373270	UVX	0.066
XMMSL1 J192404.3+552933	Y	0.39±0.17	291.0198	55.4939	GALEX J192404.7+552937	QSO	-
XMMSL1 J194240.3-101919	Y	2.58±0.65	295.6691	-10.3236	NGC 6814	Sy1	0.0052
XMMSL1 J201117.1+600431	Y	1.14±0.30	302.8201	60.0744	GALEX J201116.8+600428	QSO	-
XMMSL1 J202931.2-614858	-	0.62±0.20	307.3801	-61.8191	PGC 352109	Gal	0.19
XMMSL1 J204142.3+185258	Y	1.25±0.40	310.4283	18.8842	GALEX J204142.8+185303	QSO	-
XMMSL1 J204206.1+242653	Y	0.78±0.27	310.5252	24.4479	1RXS J204206.3+242655	BLLac	0.102
XMMSL1 J204236.3+240615	-	0.71±0.33	310.6491	24.1026	WISE J204235.78+240609.1	Gal	-
XMMSL1 J205129.5-154510	-	0.49±0.16	312.8729	-15.7533	GALEX J205129.3-154511	QSO	-
XMMSL1 J205558.4-152927	-	0.56±0.19	313.9914	-15.4914	PGC 3093850	Gal	0.08
XMMSL1 J205617.1-471450	Y	0.76±0.23	314.0681	-47.2465	B2052-474	QSO	1.489
XMMSL1 J211354.1+820450	Y	2.31±0.46	318.5048	82.0801	S5 2116+81	Sy1	0.086
XMMSL1 J211928.2+333305	Y	1.61±0.45	319.8714	33.5492	WISE J211929.13+333257.1	Gal	0.051
XMMSL1 J212434.9-113122	-	0.48±0.16	321.1449	-11.5232	1RXS J212434.7-113125	Gal	0.42

**Table A.1.** Continued

Slew ID	Soft	Flux	RA	Dec	ID	Type	Redshift
XMMSL1 J212940.5+000518	Y	0.82±0.26	322.4166	0.0894	WISE J212939.98+000521.9	Gal	0.234
XMMSL1 J213227.6+100821	Y	0.87±0.31	323.1159	10.1387	UGC 11763	Sy1	0.063
XMMSL1 J214958.0-185923	Y	0.81±0.23	327.4919	-18.9899	RXS J21499-1859	Sy1	0.158
XMMSL1 J215155.4-302755	Y	0.75±0.24	327.9813	-30.4649	B2149-306	QSO	2.345
XMMSL1 J215705.4+063222	-	0.57±0.20	329.2729	6.5381	PGC 3091877	Gal	0.115
XMMSL1 J220907.9-274843	Y	1.11±0.32	332.2820	-27.8095	NGC 7214	Sy1.2	0.023
XMMSL1 J220915.8-470954	Y	2.09±0.36	332.3175	-47.1667	NGC 7213	Sy1	0.0060
XMMSL1 J222344.1+115010	Y	0.69±0.21	335.9376	11.8359	MCG +02-57-002	Sy1.5	0.029
XMMSL1 J222547.2-045701	-	0.81±0.32	336.4469	-4.9503	4C -05.92	BLLac	1.404
XMMSL1 J222940.2-083253	Y	0.83±0.32	337.4170	-8.5484	PKS 2227-088	QSO	1.559
XMMSL1 J223248.4-202222	Y	0.63±0.18	338.2033	-20.3739	GALEX J223248.8-202225	QSO	-
XMMSL1 J223301.0+133557	Y	0.85±0.32	338.2546	13.6006	RXS J2233.0+1335	BLLac	0.213
XMMSL1 J223546.3-260301	Y	1.47±0.31	338.9425	-26.0504	NGC 7314	Sy1.9	0.0047
XMMSL1 J224641.8-520637	Y	0.85±0.24	341.6754	-52.1112	RBS 1895	BLLac	0.194
XMMSL1 J225100.7+781447	Y	0.62±0.22	342.7545	78.2445	WISE J225101.09+781440.1	Gal	-
XMMSL1 J225146.8-320613	Y	1.12±0.22	342.9481	-32.1036	RBS 1906	BLLac	0.246
XMMSL1 J225505.8-020628	-	0.99±0.39	343.7771	-2.1080	WISE J225506.50-020628.7	Gal	-
XMMSL1 J225932.6+245502	Y	0.62±0.21	344.8872	24.9184	KAZ 320	Sy1	0.034
XMMSL1 J230047.1-125513	Y	0.56±0.23	345.1992	-12.9185	NGC 7450	Sy1	0.01
XMMSL1 J230302.8-184128	Y	0.73±0.22	345.7624	-18.6905	PKS 2300-18	Sy1	0.128
XMMSL1 J230402.2+223726	Y	0.39±0.16	346.0109	22.6243	Mrk 315	Sy1	0.039
XMMSL1 J232523.8-382651	Y	1.57±0.51	351.3508	-38.4470	IRAS 23226-3843	Sy1	0.036
XMMSL1 J234333.9+343955	Y	0.82±0.30	355.8899	34.6641	SHBL J234333.8+344004	QSO	0.366
XMMSL1 J235727.7-302738	Y	1.42±0.60	359.3668	-30.4612	DUGRS 471-011	Sy1	0.03